



HAL
open science

Peroxidised phospholipid bilayers: insight from coarse-grained molecular dynamics simulations

Yachong Guo, Vladimir Baulin, Fabrice Thalmann

► **To cite this version:**

Yachong Guo, Vladimir Baulin, Fabrice Thalmann. Peroxidised phospholipid bilayers: insight from coarse-grained molecular dynamics simulations. *Soft Matter*, 2016, 12 (1), pp.263-271. 10.1039/C5SM01350J . hal-03529878

HAL Id: hal-03529878

<https://hal.science/hal-03529878v1>

Submitted on 17 Jan 2022

HAL is a multi-disciplinary open access archive for the deposit and dissemination of scientific research documents, whether they are published or not. The documents may come from teaching and research institutions in France or abroad, or from public or private research centers.

L'archive ouverte pluridisciplinaire **HAL**, est destinée au dépôt et à la diffusion de documents scientifiques de niveau recherche, publiés ou non, émanant des établissements d'enseignement et de recherche français ou étrangers, des laboratoires publics ou privés.

Cite this: DOI: 10.1039/xxxxxxxxxx

Peroxidised phospholipid bilayers: insight from Coarse-Grained Molecular Dynamics simulations

Yachong Guo,^a Vladimir A. Baulin^a, Fabrice Thalmann,^{*b}

Received Date
Accepted Date

DOI: 10.1039/xxxxxxxxxx

www.rsc.org/journalname

An original coarse-grained model for peroxidised phospholipids is presented, based on the MARTINI lipid force field. This model results from a combination of thermodynamic modelling and structural information on the area per lipid, which have been made available recently. The resulting coarse-grained lipid molecules form stable bilayers, and a set of elastic coefficients (compressibility and bending moduli) is obtained. We compare the compressibility coefficient to the experimental values [Weber *et al.*, *Soft Matter*, 2014, **10**, 4241]. Predictions for mechanical properties, membrane thickness and lateral distribution of hydroperoxide groups in the phospholipid bilayer are presented.

1 Introduction

Oxidative stress¹ plays an important role in regulating vital processes in living organisms: defense against bacteria, cell apoptosis, immune response, cell maturation and differentiation. Free radicals or reactive oxygen species (ROS)¹ may react chemically with cell constituents, leading to irreversible damage. First line of defense of cells is the cell membrane² where lipids, proteins, cholesterol, vitamins and fatty acids first interact with the external environment of the cell.

It is generally accepted^{3,4} that the protection of cell membranes from oxidation stress is due to incorporation of molecules containing weak chemical bonds (anti-oxidants): vitamins, unsaturated fatty acids, unsaturated lipids, that can break and deactivate free radicals. In particular, oxygen radicals damage weak double bond in the tails of unsaturated lipids and fatty acids, provoking changes in their conformations and disturbing the bilayer. Balanced amount of free radicals and anti-oxidants is essential for normal function of living organisms.⁵ However, when this balance is altered, it can lead to a series of diseases ranging from cancer and diabetes to several ageing diseases⁶ such as Parkinson and Alzheimer diseases.

Lipid peroxidation is a major consequence of oxidative damage to cell membranes due to various external factors^{1,3} such as reactive oxygen species (ROS), inflammation, catalysis by peroxisomal oxidases, virus phagocytosis, ultraviolet and ionic irradiation. Photooxidation of giant lipid vesicles allows to quantify

the effect of oxidation on lipid bilayers.^{7–11} In particular, with a careful choice of photosensitizer, it becomes possible to generate specifically lipid peroxides.⁹ This approach allows to control the rate of oxidation and the total area of the vesicle, providing information on the rigidity of the lipid bilayer and the variation of the area per lipid with the degree of oxidation.

In turn, lipid bilayer structure modifications due to oxidised lipids can be directly assessed with all-atoms Molecular Dynamics (MD) simulations,¹² including peroxidised polyunsaturated lipids.^{13–15} Only recently have been introduced coarse-grained (CG) model of oxidised species¹⁶ and Single Chain Mean Field (SCMF) approaches.^{9,17} According to these simulations, the increase of area per lipid, decrease of bilayer thickness and shift of peroxidised group towards the surface of the bilayer are general manifestations of oxidation.

In this paper we introduce a coarse-grained molecular model of hydroperoxidised lipids based on recent experimental data.^{9,11} Using this model we evaluate the effect of peroxidation on the thermodynamic and mechanical properties of fully peroxidised lipid bilayers.

Coarse-grained models have been widely used to describe the structure and dynamic properties of lipid bilayers providing good pictures of self-assembly of lipid bilayers and collective phenomena.¹⁸ One of the most widely employed coarse-grained model of lipid bilayers for molecular dynamics simulations is the MARTINI force field,¹⁹ which gives realistic structure and elastic properties of lipid bilayers. Thus, we use this model as a starting point for peroxidised phospholipid molecules.

^a Departament d'Enginyeria Quimica, Universitat Rovira i Virgili 26 Av. dels Països Catalans, 43007 Tarragona, Spain

^b Institut Charles Sadron, CNRS and University of Strasbourg, 23 rue du Loess, F-67034 Strasbourg, France. Fax: 33 388414099; Tel: 33 388414097; E-mail: thalmann@ics.u-strasbg.fr

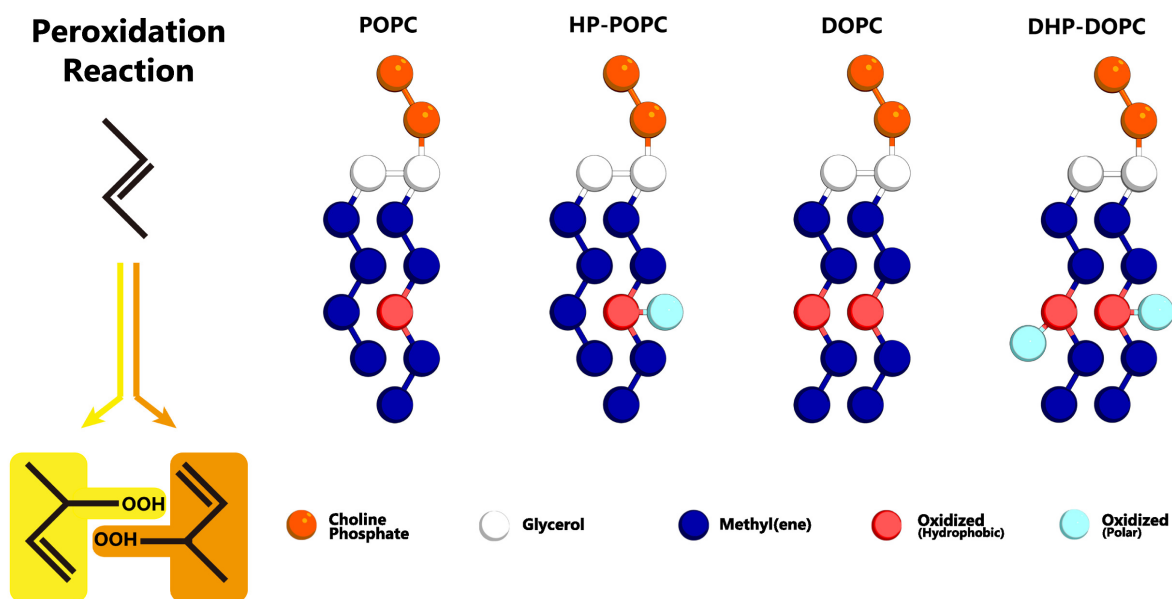


Fig. 1 Left: addition of reactive singlet oxygen to a chain unsaturation. Right: oxidised lipid molecules based on MARTINI coarse-grained models for POPC and DOPC phospholipids: HP-POPC and DHP-DOPC respectively. Bead types without exception are already present in the MARTINI model,¹⁹ without change of the mutual interaction parameters.

Lipid	Box area (nm ²)	Box thickness (nm)	Box volume (nm ³)
POPC	163.9 ± 0.2	6.551 ± 0.004	1072.04 ± 0.04
HP-POPC	190.8 ± 0.3	5.821 ± 0.006	1110.63 ± 0.04
DOPC	171.48 ± 0.13	6.576 ± 0.005	1127.67 ± 0.04
DHP-DOPC	204.92 ± 0.4	5.87 ± 0.02	1203.55 ± 0.05

Table 1 Simulation box properties for symmetric bilayers with 512 lipids and 3072 CG water beads, at 1 bar and 300 K.

2 Coarse-grained models of hydroperoxidized lipids

We construct oxidised lipid models based on the original MARTINI models¹⁹ for 1-palmitoyl-2-oleoyl-sn-glycero-3-phosphocholine (POPC) and 1,2-dioleoyl-sn-glycero-3-phosphocholine (DOPC) phospholipid molecules. We assume that hydroperoxidation acts on the double bond in the tail, C=C, resulting in a shift of its position and the addition of a side -OOH group. Further oxidation damage to lipids may cause chain cleavage and severe lipid degradation, which we do not consider in the present study.

MARTINI coarse-graining strategy is based on a 4 atoms to 1 bead correspondence,¹⁹ with effective potentials between beads accounting for the thermodynamic mixing properties of the underlying molecular sub-groups. Hydroperoxidation has the effect of adding two oxygen atoms to an existing group of 4 carbons (Fig. 1) as a result of so-called Type II photooxidation reactions.^{22,23} The CG model must therefore account for 6 atoms with amphipathic properties.

We consider that the two peroxidised products are indistinguishable at the coarse-grained level adopted here, and assume that both can be suitably represented by a single assembly of beads with average properties. The hydrophobic part retains an unsaturated C=C bond, as in the original target. The hydrophilic

part OOH is without doubt a polar group with donor and acceptor hydrogen bonding character. The 6 atoms group C₄OOH is bulkier than the original unoxidised group C₄. One could imagine introducing for that a larger bead, but it would then be necessary to reimplement all the pairwise Lennard-Jones interactions with the other existing coarse-grained beads. Then, a bead of intermediate polarity can only poorly reproduce the two-sided (hydrophobic-polar) character of C₄OOH. At the opposite, a set of two beads (dimer) can optimally traduce the intrinsic amphipathy of the group. By adjusting the separation between beads, as in the case of the glycerol backbone, the bulkiness of the pair can be set to a reasonable value, 50% higher than the original C₄ group (6 atoms instead of 4).

Our systematic investigations lead us to the conclusion that an optimal choice is the adjunction of MARTINI C3 (hydrophobic) bead to a MARTINI P2 (polar, h-bonding donor and acceptor) bead, separated by 0.33 nm, smaller than the standard lipid bonding distance (0.47 nm). Note that the structural properties of the resulting bilayer depend quite sensitively on this separation. This choice, as explained in Section 4, comes from a comparison with the experimental change in area per lipid resulting from the complete hydroperoxidation of the unsaturated pure POPC and DOPC lipid bilayers. The average increase in area per lipid following complete peroxidation is reported to be +15.6% for POPC bilay-

ers, and +19.1% for DOPC bilayers respectively.⁹ Similar area changes were also obtained by monitoring giant vesicles adhering onto specially prepared adhesive surfaces,¹¹ then leading to relative area changes of +14.3% and +18.4% for oxidised POPC and DOPC vesicles respectively. These values are fairly consistent, given the practical difficulties inherent to these experimental techniques. This combination of results puts stringent constraint on the CG candidate models.

Mapping to this structural quantity, however, is no substitute for performing a thermodynamic mixing assay of the C₄OOH target group. For this purpose, knowing the chemical structure of the oxidised lipid, we selected tert-butyl hydroperoxide (TBHP, CAS 75-91-2, a commercial bleaching agent)²⁴ as the best analogue to the peroxidised functional group C₄O₂. The values of water solubility and octanol/water partitioning log *P*_{ow} data of TBHP we could find are scattered between 0.6 and 1.23, while simulations of the C3-P2 dimer alone suggest a numerical, coarse-grained log *P*_{ow} = 1.4. Finally, the acidic constant of TBHP, *pK*_a = 12.8, suggests a predominantly protonated, neutral hydroperoxide group, for neutral or slightly acidic pH solutions.

In what follows, we designate by HP-POPC the hydroperoxidised POPC molecule, and by DHP-DOPC the doubly hydroperoxidised DOPC (Fig. 1). We find that bilayers formed with pure HP-POPC and DHP-DOPC are stable, and provide a set of numerically estimated structural and mechanical parameters, associated with these two lipid bilayers. Snapshots of bilayers formed with POPC, DOPC, HP-POPC and DHP-POPC are provided in Fig. 2.

3 Results and discussion

3.1 Structural changes upon peroxidation

Pure HP-POPC and DHP-DOPC bilayers appear numerically stable and lend themselves to the determination of fairly precise structural properties. The main structural data are summarized in Table 1. Area per lipid was used to set up CG models. Assuming that these values are correct, resulting CG models provide a quantitative estimate of membrane thickness and membrane specific volume changes due to peroxidation. If one assumes that membranes are quasi-incompressible media, the volume change is entirely due to the added hydroperoxide groups, and it becomes possible to split the increase in area per lipid into two contributions: homogeneous increase and structural reorganisation. The homogeneous increase of area is directly proportional to the relative volume change $(\Delta A/A)_{hom} = 2/3(\Delta V/V_b)$, as if the bilayer was an homogeneous fluid with volume *V*_b. The second contribution is due to the membrane reorganisation due to changes in chemical affinity and polarity following the addition of the hydroperoxide groups. The corresponding “structural” relative increase of area is $(\Delta A/A)_{str} = \Delta A/A - (\Delta A/A)_{hom}$.

Lipids were simulated in a box with lateral *x, y* directions and transverse *z* direction, at a temperature of 300 K. An anisotropic Parinello-Rahman barostat was applied to simulate a tensionless bilayer (all three directions being subject to a 1 bar compressive stress), and the average lateral size $L_x = L_y$ of the system provides the desired bilayer area $A = \langle L_x L_y \rangle$. Changes in membrane volume and membrane thickness upon peroxidation are obtained

by monitoring the changes in the average simulation box volume $\langle L_x^2 L_z \rangle$ and lateral extension $\langle L_z \rangle$.

The area of the simulation box and the area of the bilayer can be considered equal, as the excess area caused by undulations is small, especially for systems comprising only 512 lipids. There is however a significant difference between the volume and thickness of the box compared with the volume and thickness of the bilayer only. Let us denote by *V*_b and *L*_b the volume and lateral thickness of the bilayer, and by *V* and *L*_z the volume and thickness of the simulation box mentioned in Table 1. The simplest way to relate *V* and *V*_b or *L*_z and *L*_b consists in removing the volume of the homogeneous solvent taken at same pressure and temperature. The volume of 3072 CG fluid water system is $V_s = 366.04 \pm 0.07 \text{ nm}^3$. The bilayer volume and thickness follows from the expressions

$$V_b = V - V_s; L_b = L_z - \frac{V_b}{A}. \quad (1)$$

Such an approximation means that change in water structure at the vicinity of bilayers are disregarded, and is known as the Luzzati approximation.²⁵

The resulting bilayer volumes and thicknesses are summarised in Table 2 below. Upon peroxidation, the volume change of the bilayer coincides with the volume change of the simulation box. Relative volume, thickness and area changes are summarised in Table 3. We notice in particular that the structural area variations $(\Delta A/A)_{str}$ are almost identical for both oxidised lipids. The higher density of hydroperoxide groups in DHP-DOPC compared with HP-POPC does not lead to an increase in area per lipid beyond a trivial change in bilayer volume *V*_b.

3.2 Hydroperoxide group distribution

The CG models give also a prediction for lateral density profiles, and in particular for the hydroperoxide group distribution. The partitioning of C₄OOH between the water interface and the inner hydrophobic region obey a subtle statistical balance. On the one hand the group must show affinity for the interfacial water, on the other hand, the h-bonding donor and acceptor character promotes self-interaction.

The density distribution of an equilibrated coarse grained DHP-DOPC bilayer and HP-POPC bilayer is shown in Fig. 3. Both density distributions were obtained from a simulation of a bilayer patch containing 512 DHP-DOPC/HP-POPC lipids at full hydration (6 CG water beads equivalent to 24 water molecules per lipid) at room temperature (*T* = 300 K) with the lateral and normal pressures independently coupled to a pressure of 1 bar. The local center of the bilayer was calculated and used in the present work to determine the density as follows: the *xy* plan of the simulation box was divided into 8 × 8 regions, and the local positions of the bilayer center were calculated as $\bar{z} = \langle z \rangle$, where the averaging was performed over all lipid monomers in the given region. This position was further used in binning the density profile to shift the bilayer center.

The hydroperoxide group is represented by two connected beads, one hydrophobic (C3) referred as hydrophobic oxidised

	POPC	HP-POPC	DOPC	DHP-DOPC
Thickness (nm)	4.318 ± 0.006	3.90 ± 0.01	4.442 ± 0.007	4.08 ± 0.03
Area (nm ²)	163.9 ± 0.02	190.8 ± 0.3	171.48 ± 0.13	204.9 ± 0.4
Volume (nm ³)	706.02 ± 0.08	744.61 ± 0.08	761.65 ± 0.08	837.53 ± 0.09
Area/lipid (nm ²)	0.6402 ± 0.0008	0.7453 ± 0.0012	0.6698 ± 0.0006	0.8005 ± 0.0016
Volume/lipid (nm ³)	1.3789 ± 0.0002	1.4542 ± 0.0002	1.4875 ± 0.0002	1.6357 ± 0.0002

Table 2 Equilibrium bilayer thickness, area, volume, area per lipid and volume per lipid of POPC and DOPC phospholipids, and corresponding oxidised analogs HP-POPC and DHP-DOPC (512 lipids systems).

Lipid	Volume	Area	Thickness	$(\Delta A/A)_{str}$	Weber <i>et al.</i>
POPC	5.46%	16.4%	-9.6%	12.8%	15.6%
DOPC	9.96%	19.5%	-8.1%	12.9%	19.1%

Table 3 Relative structural changes of the bilayer following peroxidation of POPC and DOPC molecules. The last column represents the experimental changes in area per lipid reported by Weber *et al.*⁹

and one hydrophilic (P2) referred as polar oxidised, kept at a relative distance of 0.33 nm. The distribution of the polar oxidised beads, representing the OOH side group, is naturally wider than its hydrophobic counterpart which belongs to the lipid tail backbone. A bimodal distribution is seen in both cases. Roughly half of the polar oxidised beads overlap with the glycerol group in the case of HP-POPC, with the other half remaining “buried” at the same place as the corresponding beads of the opposite saturated lipid tails (Fig. 3 above). By comparison, only a quarter of the polar oxidised beads in DHP-DOPC occupy a region close to the glycerol part, the other three quarters staying deep into the hydrophobic region (Fig. 3 below). As DHP-DOPC has twice as many oxidised groups as HP-POPC, it seems that all the extra oxidised beads go into the hydrophobic core of the bilayer, and that the interfacial glycerol region cannot take more oxidised groups than it has in the HP-POPC case. This is consistent with the data in Table 3 suggesting that the structural increase in area per lipid is similar for both species.

Fig. 4 depicts the orientational distribution of the packing angles: the angle between oxidised tail and z -axis α and the angle between two tails of the lipid β . Both DHP-DOPC and HP-POPC have a similar distribution of α , though, judging from the wider distribution, HP-POPC has a larger averaged angle than DHP-DOPC. Peroxidised lipids are therefore significantly tilted with respect to the bilayer normal.

The angle β is defined as the angle between oxidised bead, glycerol bead and mirror alkyl bead in the opposite tail. We find a wide distribution of β for DHP-DOPC with a peak value around 68°. In turn, the angle distribution of β for HP-POPC is narrower with its peak value around 51°. The packing angle β is closely related to the effective shape of a lipid molecule and thus it determines the ability of lipids to form a stable bilayer. Wide angles correspond to larger deviations from cylindrical shape, possibly resulting into less stable bilayers.

3.3 Elasticity of hydroperoxidised bilayers

The membrane compressibility (or stretching modulus) K_A gives the relative area (A) variation consecutive to applied tension (σ), according to the definition²⁵:

$$K_A = \frac{1}{A} \left(\frac{dA}{d\sigma} \right)_{T,P}. \quad (2)$$

The stretching modulus can be experimentally determined by micropipette aspiration.²⁶ Values of K_A for DHP-DOPC and HP-POPC were published first by Weber *et al.*⁹ and are summarised in the Table 4.

The elastic coefficients K_A associated to our coarse-grained numerical models come from an area fluctuation analysis, according to the equilibrium statistical relation

$$K_A = \frac{k_B T \langle A \rangle}{\langle A^2 \rangle - \langle A \rangle^2} = \frac{k_B T}{4(\langle L_x^2 \rangle - \langle L_x \rangle^2)}, \quad (3)$$

with $\langle A \rangle$ and $\langle A^2 \rangle$ the mean value and the quadratic fluctuation of the sample monolayer area $A = L_x L_y$, and $\langle L_x \rangle$, $\langle L_x^2 \rangle$ the mean value and quadratic fluctuation of the lateral size of the anisotropic simulation box. The fluctuations of area result from coupling the system to a semi-isotropic Parrinello-Rahman barostat²⁸, known to generate the adequate constant pressure box size fluctuations. It can be shown that the elastic coefficient determined in this way is consistent with the one obtained by exerting an change in lateral stress (tension) on the membrane. The uncertainties quoted in Table 4, are associated with the precision to which $\langle L_x^2 \rangle - \langle L_x \rangle^2$ is determined.

Numerical estimates of K_A notoriously depend on sample size.²⁰ According to den Otter, larger samples appear softer due to long wavelength undulation modes, whose contributions can be accounted for analytically in the relevant limit.²¹ Using this analytical relation (*cf* section 4) a better, undulation-free estimate of the membrane compressibility can be inferred, based on the apparent K_A corresponding to two different sample sizes.

We report in Table 4 our values obtained for 512 (small) and 8192 (large) lipid samples, along with the undulation free extrapolation. For DOPC and POPC bilayers, the MARTINI CG model overestimates the accepted experimental values, while large samples (*e.g.* 8192 lipids in our case) show a (coincidental) better agreement with them. We assume the same trend holds for the hydroperoxidised bilayers. Our investigations suggests that hydroperoxidation leads to a significant decrease of K_A in both POPC and DOPC cases, whether the simulated system is small or large. This decrease of K_A upon peroxidation appears therefore like a

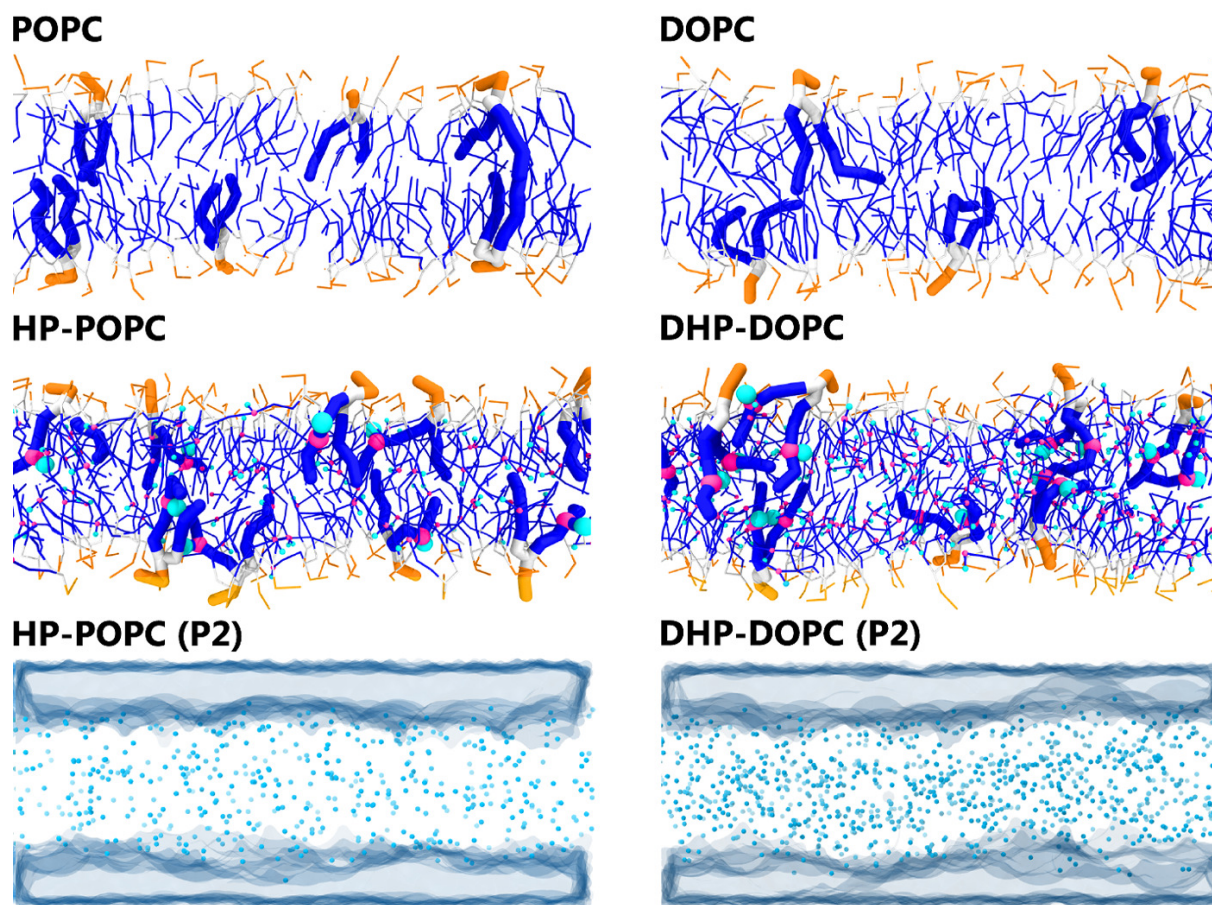


Fig. 2 Snapshots of the 512 lipid samples: top and middle rows. Distribution of the polar oxidised beads and water regions in HP-POPc bilayers (bottom left) and DHP-DOPc (bottom right).

robust and significant trend.

The membrane bending modulus coefficient κ_b controls the out-of-plane bending deformation of a membrane in the Canham-Helfrich elastic model.²⁹ It can be determined experimentally by a number of techniques, including micropipette vesicle aspiration, vesicle flicker motion and nanotube pulling, but unfortunately we are not aware of any published values of κ_b to date. We therefore take our values as predictions.

The numerical determination of the bending modulus requires to deal with simulated systems of sufficient size corresponding to a small ratio L_b/L_x between the membrane thickness and the lateral extension. Only under these conditions does the continuous Helfrich elastic model bring a reasonable description of the out-of-plane membrane fluctuations. Our determination of κ_b is based on the equilibrium fluctuation analysis of samples comprising 8192 lipids. Larger systems would approach better the Helfrich continuous limit, but equilibration times tend to increase sharply due to a combination of weak restoring forces and hydrodynamic effects, in spite of the parallel computation capabilities of the simulation tools.

In the continuum model, the bending modulus appears in the quadratic out-of-plane fluctuations spectrum $\langle u(q)u(-q) \rangle$, where q is the wavevector parallel to the membrane plane, and $u(x,y)$ the out-of-plane displacement in the Monge representation (elevation

of the continuous surface):

$$\langle u(q)u(-q) \rangle = \frac{k_B T}{\kappa_b} \frac{1}{\langle A \rangle q^4}. \quad (4)$$

Numerical simulations do not provide $u(x,y)$ directly, and there is a certain arbitrariness when it comes to determining $u(x,y)$ from the discrete beads representation of the lipid molecules. At the molecular scale, each lipid fluctuates around the average bilayer position, due to tilt, protrusion and other possible movements. This gives extra-contributions to the structure factor of the bilayer, and eqn (4) is not expected to hold exactly.³⁰ At smaller q , however, eqn (4) should hold for tensionless bilayers.

We derive our numerical estimate of the bending moduli by fitting $\langle U(q)U(-q) \rangle$ to a q^{-4} behaviour, where $U(q)$ is a discrete beads estimate of the elevation field $u(q)$ ³¹ (see Fig. 6 and Section 4 for details). Our predictions for κ_b are summarised in Table 5. As for the area compressibility (or stretching) coefficient, hydroperoxidation causes a sharp decrease in the bending modulus value. As a result, the elastic bending forces are weaker, and the bilayer undulation dynamics slower.

The POPc, HP-POPc and DOPc undulation spectra all follow the Helfrich q^{-4} behaviour, while DHP-DOPc undulations does not comply with it so well, showing a weaker apparent exponent. This might be due to DHP-DOPc molecules not fitting perfectly

	K_A (mN/m) 512 CG model	K_A (mN/m) 8192 CG model	K_A (mN/m) undulation free	K_A (mN/m) experimental
POPC	379. \pm 21.	245. \pm 42.	393. \pm 25.	230. \pm 10.
HP-POPC	211. \pm 11.	104. \pm 25.	227. \pm 16.	\sim 50.
DOPC	357. \pm 19.	230. \pm 27.	371. \pm 22.	265. \pm 18.
DHP-DOPC	103. \pm 12.	73. \pm 7.	106. \pm 14.	\sim 50.

Table 4 Stretching moduli of POPC, HP-POPC, DOPC, DHP-DOPC. Experimental results for POPC and DOPC bilayers are taken from Rawicz et al.,²⁶ and for HP-POPC and DHP-DOPC from Weber et al.⁹

	κ_b ($k_B T$) CG model	κ_b (10^{-20} J) CG model	κ_b (10^{-20} J) Experimental
POPC	30.0 \pm 1.5	12.4 \pm 0.7	9.0 \pm 0.6
HP-POPC	15.1 \pm 0.9	6.3 \pm 0.4	–
DOPC	28.3 \pm 1.5	11.7 \pm 0.7	8.5 \pm 1.0
DHP-DOPC	12.8 \pm 1.2	5.3 \pm 0.5	–

Table 5 Bending moduli of POPC, DOPC, hydroperoxidised POPC and DOPC molecules. Experimental data are taken from Rawicz et al.²⁶

	D ($\mu\text{m}^2/\text{s}$) CG model	D ($\mu\text{m}^2/\text{s}$) Experimental
POPC	40.2 \pm 2.6	4.2 \pm 0.4
HP-POPC	32.2 \pm 2.2	–
DOPC	34.5 \pm 1.5	6.3 \pm 0.2
DHP-DOPC	24.4 \pm 2.2	–

Table 6 Diffusion coefficients of the numerical CG lipids. Experimental values comes from ref.²⁷ Coarse-graining molecular dynamics is always faster than reality by a significant factor. Only relative trends may be of significance.

into the bilayer structure.

3.4 Relative changes in diffusion coefficients

We have estimated the diffusion coefficient of each lipid, at 300 K, using the MARTINI coarse-grained dynamics. It is known that coarse-graining predicts faster diffusion than experimentally observed. The extent of the acceleration factor, depending on temperature, may lie between 4 and 10. We observe that the hydroperoxidised lipids diffuse slower than the non-oxidised molecules by roughly 25%. This suggests an increased cohesion between peroxidised molecules, but only by a modest amount.

The lateral diffusion coefficient was calculated from the mean-square displacement (MSD) of lipid centres of masses with time. The resulting MSD curves are linear, to a good approximation, over a time interval between 20 and 50 ns (simulation time). Lateral diffusion coefficients were obtained from linear fits of these MSD curves between 20 and 50 ns.

According to Table 6 and Fig. 5, the lateral diffusion coefficient decreases due to lipid oxidation, and we observe that the diffusion coefficient ratio between the oxidised and the non-oxidised species is similar in both cases: 0.77 for HP-POPC/POPC and 0.76 for DHP-DOPC/DOPC. The decrease in diffusion coefficient could arise from a larger friction at the water-bilayer interface, or from stronger lipid-lipid interaction, due to attractive patches in the

tails at the position of the peroxide groups. The former interpretation is more consistent with the common 25% drop in value.

Two experimental values, based on fluorescent probes diffusion, are provided to show the expected order of magnitude of the ratio between CG simulated and experimental time scales²⁷. This choice is somewhat arbitrary, as a large number of experimental diffusion coefficients values are available, which differ greatly depending on the technique and system preparation. Coarse-Grained models do not perform very well as far as reproducing dynamics and transport properties³². We see a reduction of lipid mobility upon peroxidation that seems due to increased friction between peroxidized groups and interfacial water. It might be that important dynamical changes, which are not be accounted for in our approach, alter the overall picture.

4 Simulation and analysis details

4.1 Parameterisation of the CG hydroperoxidised lipids

A first attempt was made by substituting one hydrophobic bead with an hydrophilic bead. Based on $\log P_{ow}$, we find that a moderately hydrophilic bead does not account for the observed area change. Conversely, significant area increase can only be obtained for strongly hydrophilic beads which violate the $\log P_{ow}$ requirement. The partition coefficient and the increase in area per lipid can be reconciled by modelling the hydroperoxide group as two partially overlapping beads. A systematic screening was performed with pairs of beads with different polarities (C1 till C3, and P1 till P4) and separations (0.3 till 0.4 nm) and compared to the experimental area per lipids of both HP-POPC and DHP-DOPC. Two dimers (C2-P2) and (C3-P2) emerged as the best contenders based on both partitioning and area per lipid criteria. Both could be used with little changes in the results and we picked-up C3-P2 as reference dimer. To give an idea on how much bead separation affects the area per lipid, we note that a distance 0.32 nm would give area changes of +15.8% (HP-POPC) and +17.7% (DHP-DOPC), as compared with values in Table 3, obtained for 0.33 nm.

Most MARTINI CG beads have a Van der Waals radius $\sigma=0.47$ nm, so that a dimer made of two beads at distance $r=0.33$ nm gives an excluded volume 50% larger than a single bead. More precisely, if the beads were hard spheres, the combination of two hard spheres of radius 0.47 separated by 0.33 gives a total excluded volume equal to 1.505 times the excluded volume of a single sphere. A direct consequence is that the volume per lipid increases by respectively 5.5% and 10% for POPC and DOPC. No bending potential was added between the C3-P2

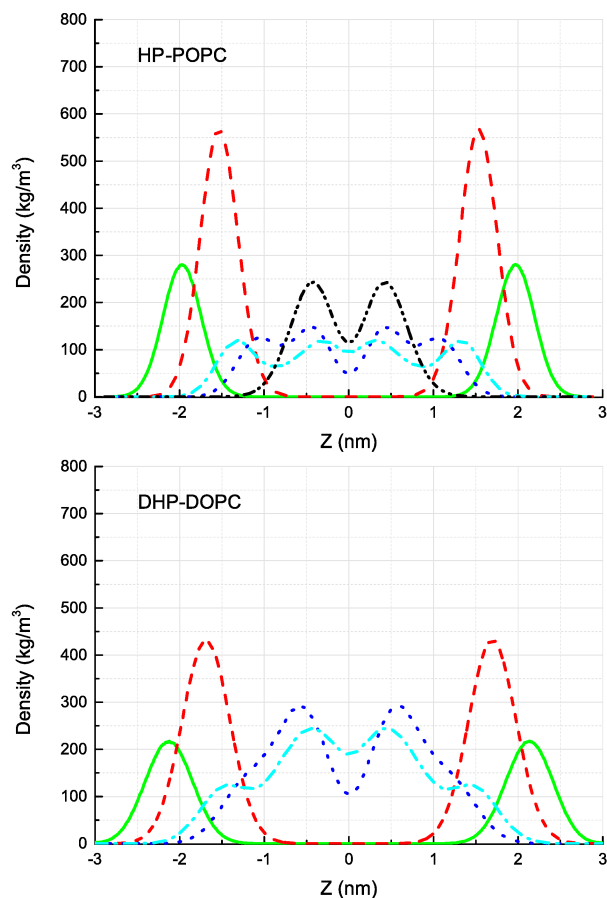


Fig. 3 Partial mass densities for HP-POPC (top) and DHP-DOPC (bottom) phosphate group (Green/full line), glycerol (Red/dashed line), Hydrophobic Oxidised (Blue/dotted line), Polar Oxidised (Cyan/dash-dotted line), 3rd hydrophobic group (C3A in the Martini model of POPC) of the opposite saturated tail of POPC (Black/dash-dot-dotted line). The bilayer center lies at $z = 0$ nm.

bond and the remaining of the lipid chain. Steric interactions ensures that the polar moiety P2 remains at distance from the chain, and additional structural information is lacking to improve over the current parameterisation. One must remember also that our CG model stands for a chemical mixture of at least two chemical compounds, for which the *cis* or *trans* nature of the unsaturated double bond is not established even though a majority of *trans* bonds is expected.

Partitioning of the corresponding C3-P2 dimers was carried out by studying a slab of 1920 octanol molecules (MARTINI “OCO” dimers) surrounded by 2000 “water molecules” (one CG water representing 4 real water molecules), in which 40 dimers were inserted. The concentration ratio was found to be $P_{ow} = [C3P2]_{oct}/[C3P2]_w = 26$, or equivalently $\log P_{ow} = 1.4$. This can, for instance be compared with the estimated $\log P_{ow} = 0.9$ of tert-butyl hydroperoxide ((CH_3)₃COOH, CAS-75-91-2), obtained using with a $\log P_{ow}$ predicting software (VCCLab³³). This indicates that our residue C3-P2 has a realistic hydrophilic-hydrophobic balance.

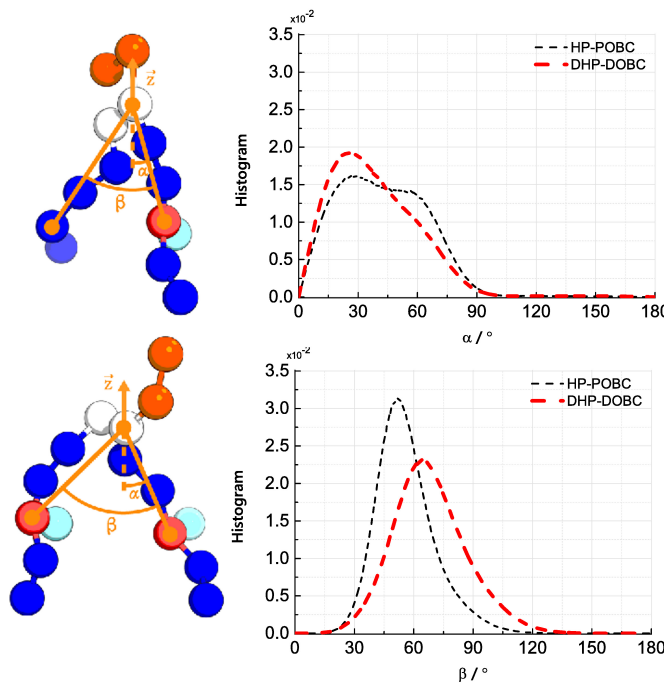


Fig. 4 Left) Definition of the tilting and opening angles α and β . Right) Distribution of orientations of α and β for HP-POPC and DHP-DOPC.

4.2 Stability of peroxidised bilayers

Bilayers composed of single components HP-POPC and DHP-DOPC are stable, to the extent that systems composed of pure HP-POPC and DHP-POPC exhibit stationary properties and show no significant evolution over the simulated times. In practice, initial configurations are obtained by starting from thermalized POPC and DOPC bilayers, inserting the extra beads and reequilibrating again the systems.

4.3 Simulation details

This CG model of peroxidised lipids is built on the version 2.0 of MARTINI lipid molecules topologies, and the version 2.1 of the bead interaction parameters. Trajectories were produced using Gromacs v-4.6.

Simulations were carried out at constant temperature (300 K) using the Gromacs *v-rescale* weak coupling scheme, which is an alternative to *Nose-Hoover* thermostating (time constant 1 ps).³⁴ Anisotropic Parrinello-Rahman barostat was used to model a tensionless bilayer (time constant 12 ps, compressibility $3 \times 10^{-4} \text{ bar}^{-1}$). Simulation box size fluctuations are assumed to be consistent with a constant Temperature-Pressure ensemble, and were used as such for the determination of the membrane area compressibility coefficient.

Short range electrostatics is assumed, with truncation at a radius of 1.2 nm, while the Verlet neighbour list radius was set to 1.4 nm. Time steps of 30 fs and 40 fs were used throughout, in the absence of rigid constraints, without noticeable differences in the output. Simulation times are summarized in Table 7.

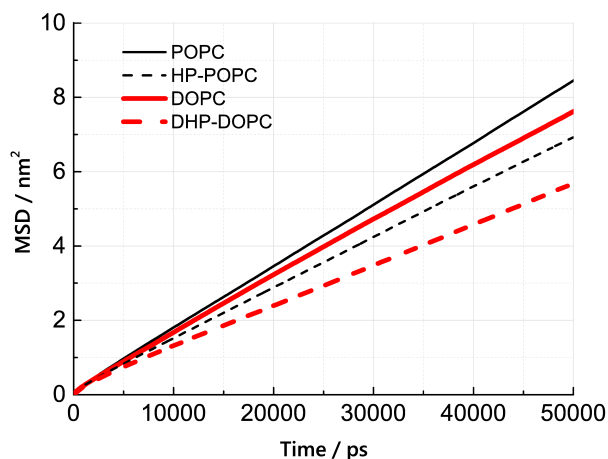


Fig. 5 Mean lateral displacements $\Delta x^2 + \Delta y^2$ versus time, for the four kinds of lipids.

Lipids	MD Steps, $\times 10^6$	CG time (ns)
512 POPC	10	400
512 DOPC	10	400
512 HP-POPC	20	800
512 DHP-DOPC	20	800
8192 POPC	20	600
8192 DOPC	20	600
8192 HP-POPC	40	1200
8192 DHP-DOPC	30	900

Table 7 Trajectories used for the determination of structural parameters.

4.4 Size dependence of the elastic compressibility coefficient

Eq. (14) in ref²¹ relates the apparent compressibility $K_{A\parallel}$ to the undulation free compressibility K_A , given the system projected area A_{\parallel} and the membrane bending modulus κ . It reads

$$K_{A\parallel}^{-1} = K_A^{-1} + \frac{k_B T}{32\pi^3 \kappa^2 A_{\parallel}}. \quad (5)$$

This expression assumes a Canham-Helfrich elastic behaviour, and account for modes of wavelength $2\pi/\sqrt{A_{\parallel}} < q < 2\pi/\lambda$, with λ a characteristic length of the size of the membrane thickness. If $K_{A\parallel,1}$ and $K_{A\parallel,2}$ are known for two different projected areas $A_{\parallel,1}$, $A_{\parallel,2}$, one can extract an effective bending modulus κ and derive K_A from eq. (5)

$$\left(\frac{\kappa}{k_B T}\right)^2 = \frac{1}{32\pi^3 k_B T} \left(\frac{A_{\parallel,1} - A_{\parallel,2}}{K_{A\parallel,1}^{-1} - K_{A\parallel,2}^{-1}}\right) \quad (6)$$

This is a less accurate estimate of κ than fitting the undulation spectrum to a Helfrich q^{-4} law, as (5) considers modes $q \sim 2\pi/\lambda$ which may deviate from the ideal Helfrich behaviour. The values of κ found in this way are nevertheless reasonably similar to those determined directly, namely 30 kT (POPC), 28.3 kT (POPC), 15.1 kT (HP-POPC) and 12.8 kT (DHP-DOPC). This is 50% larger than values in Table 5, except for DHP-DOPC for which the agreement is better. The related undulation free K_A coefficients are

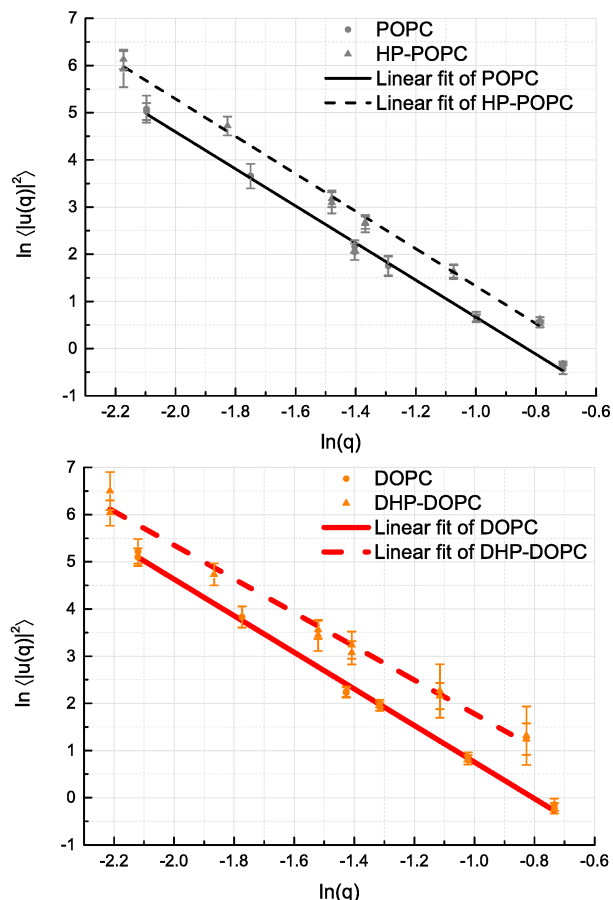


Fig. 6 Log-scale representation of the out-of-plane fluctuations of the bilayers. Only $q \leq 0.35$ [$\ln(q) \leq -1.05$] values were used for fitting the q^{-4} behaviour (q in nm^{-1} unit). Deviation from a q^{-4} behaviour can be seen in the DHP-DOPC case, which is the softer among all bilayers.

shown in the third column of Table 4.

4.5 Fitting and estimation of errors

Averages of the area, simulation box volume and thickness comes from the thermodynamic data recorded during the simulations, and Gaussian confidence intervals on the sampled means were obtained by using a bunching/boxing algorithm for time-correlated time sequences.³⁵ The statistical precision on these quantities is very satisfactory.

The bunching algorithm was also used to estimate the accuracy of the sample variance of the statistical L_x time sequence. This lead to larger uncertainties for the compressibility coefficients K_A . In the case of the undulation free K_A , uncertainties on $K_{A\parallel}$ dominates the final error.

Modes $U(q,t)$ reflects the Fourier transform of the centre of masses density field. Let us denote (x_i, y_i, z_i) the space coordinate of the centre of mass of each lipid molecule in one of the bilayer leaflet, and N_l the number of lipids in this leaflet. The density

field in reciprocal space is given by

$$\begin{aligned}\hat{\rho}_{\vec{q}} &= \frac{1}{N_l} \sum_{i=1}^{N_l} \exp(iq_x x_i(t) + iq_y y_i(t) + iq_z z_i(t)) \\ &= \frac{1}{N_l} \sum_{i=1}^{N_l} \exp(iq_x x_i(t) + iq_y y_i(t)) [1 + iq_z z_i(t)] \\ &= \hat{\rho}_{\parallel}(t) + iq_z U(q, t)\end{aligned}\quad (7)$$

We therefore simply assume that $u(q_x, q_y) \simeq U(q_x, q_y) = N_l^{-1} \sum_i z_i \exp(iq_x x_i + iq_y y_i)$. The undulation modes spectra $\ln(\langle U(q_x, q_y) U(-q_x, -q_y) \rangle)$ were fitted to straight lines $C - 4 \ln(q)$; $q = \sqrt{q_x^2 + q_y^2}$, with uncertainties resulting from a standard χ_2 least-squares procedure.³⁶

A similar estimate of the values and confidence intervals for the diffusion coefficients was used, based on the average and variance of the quadratic displacement time signal $S(t, \tau)$ of the lipid centers of masses, with respect to t , for fixed τ .

$$S(t, \tau) = \frac{1}{N} \sum_i (x_i(t + \tau) - x_i(t))^2 + (y_i(t + \tau) - y_i(t))^2. \quad (8)$$

5 Conclusion

We presented a coarse-grained model for two hydroperoxidised phospholipids based on the MARTINI force field for POPC and DOPC. The parameters of our coarse-grained molecules were set by combining thermodynamic data (the TBHP partitioning coefficient), molecular packing arguments (the addition of OOH group) and area per lipid changes.

The resulting molecules, HP-POPC and DHP-DOPC, form stable bilayers on accessible simulation times. Our results suggests that the excess area per lipid caused by peroxidation is common to both species, about 13% in relative value. The hydroperoxidised bilayers are thinner and softer than their non oxidised counterparts. A significant drop in compressibility (stretching) coefficient K_A is observed, qualitatively similar to experimental values. A similar drop of the bending coefficient κ_b is predicted. The diffusion coefficient of the coarse-grained hydroperoxidized lipids shows a 25% decrease as compared with the non-oxidised ones.

Using our model, we derive the lateral distribution of peroxide groups in the bilayers, and gain access to various structural data, such as variation of area per lipid, density profile, compressibility and bending moduli, diffusion coefficient of lipids. We hope that new experimental results will appear in a close future that can be compared to the picture presented above.

A question of interest concerns mixtures of regular and peroxidised lipid species, and in particular the possible non-ideal features of such systems. The presence of heterogeneities, if established, would be an element to consider in the understanding of the physiological consequences of lipid peroxidation. We are currently working into this direction, with the help of these newly introduced lipid models.

6 Acknowledgment

Authors acknowledge funding from Marie Curie Actions under EU FP7 Initial Training Network SNAL 608184. F.T. and Y.G. thanks the Strasbourg High Performance Cluster Equip@Meso for providing computing resources. Y.G would like to express his special thanks to Dr. Olivier Benzerara in Institut Charles Sadron, Strasbourg, France for all the discussion and help. F.T. acknowledges discussions with V. Knecht, M. Batista, A.P. Schroder and C.M. Marques.

References

- 1 R. Kohen and A. Nyska, *Toxicol. Pathol.*, 2002, **30**, 620–650.
- 2 B. Alberts, A. Johnson, J. Lewis, M. Raff, K. Roberts and P. Walter, *Molecular Biology of the Cell*, Garland Science, 4th edn, 2002.
- 3 M. Repetto, J. Semprine and A. Boveris, *Lipid Peroxidation*, InTech, 2012.
- 4 B. Frei, *The FASEB Journal*, 1999, **13**, 963–964.
- 5 D. J. Betteridge, *Metabolism.*, 2000, **49**, 3–8.
- 6 S. I. Liochev, *Free Radic. Biol. Med.*, 2013, **60**, 1–4.
- 7 K. A. Riske, T. P. Sudbrack, N. L. Archilha, A. F. Uchoa, A. P. Schroder, C. M. Marques, M. S. Baptista and R. Itri, *Biophys. J.*, 2009, **97**, 1362–1370.
- 8 O. Mertins, I. O. Bacellar, F. Thalmann, C. M. Marques, M. S. Baptista and R. Itri, *Biophys. J.*, 2014, **106**, 162–171.
- 9 G. Weber, T. Charitat, M. S. Baptista, A. F. Uchoa, C. Pavani, H. C. Junqueira, Y. Guo, V. A. Baulin, R. Itri, C. M. Marques and A. P. Schroder, *Soft Matter*, 2014, **10**, 4241–4247.
- 10 S. Sankhagowit, S.-H. Wu, R. Biswas, C. T. Riche, M. L. Povinelli and N. Malmstadt, *Biochim. Biophys. Acta*, 2014, **1838**, 2615–2624.
- 11 P.H.B Aoki, A.P. Schroder, C.J.L. Constantino, C.M. Marques, *Soft Matter*, Advanced Article (2015) doi:10.1039/C5SM01019E.
- 12 H. Khandelia and O. G. Mouritsen, *Biophys. J.*, 2009, **96**, 2734–2743.
- 13 V. Jarerattanachat, M. Karttunen and J. Wong-ekkabut, *J. Phys. Chem. B*, 2013, **117**, 8490–8501.
- 14 J. Wong-Ekkabut, Z. Xu, W. Triampo, I. M. Tang, D. P. Tieleman and L. Monticelli, *Biophys. J.*, 2007, **93**, 4225–4236.
- 15 J. Garrec, A. Monari, X. Assfeld, L. M. Mir and M. Tarek, *J. Phys. Chem. Lett.*, 2014, **5**, 1653–1658.
- 16 H. Khandelia, B. Loubet, A. Olżyńska, P. Jurkiewicz and M. Hof, *Soft Matter*, 2013, **10**, 639–647.
- 17 S. Pogodin and V. A. Baulin, *Soft Matter*, 2010, **6**, 2216–2226.
- 18 M. Muller, K. Katsov and M. Schick, *J. Polym. Sci. B: Polym. Phys.*, 2003, **41**, 1441–1450.
- 19 S. J. Marrink, H. J. Risselada, S. Yefimov, D. P. Tieleman and A. H. de Vries, *J. Phys. Chem. B*, 2007, **111**, 7812–7824.
- 20 S. J. Marrink, A. H. de Vries and A. E. Mark, *J. Phys. Chem. B*, 2004, **108**, 750–760.
- 21 W. K. den Otter *The Journal of Chemical Physics*, 2005, **123**, 214906.

- 22 H. Sies *Angewandte Chemie International Edition*, 1986, **25**, 1058–1071.
- 23 S. P. Stratton and D. C. Liebler *Biochemistry*, 1997, **36**, 12911–12920.
- 24 J. Sanchez and T. N. Myers, *Kirk-Othmer Encyclopedia of Chemical Technology*, John Wiley & Sons, Inc., 2000.
- 25 G. Cevc and D. Marsh, *Phospholipid Bilayers: Physical Principles and Models*, Wiley-Interscience, New York, 1st edn, 1987.
- 26 W. Rawicz, K. C. Olbrich, T. McIntosh, D. Needham and E. Evans, *Biophys. J.*, 2000, **79**, 328–339.
- 27 D. Marsh, *Handbook of Lipid Bilayers, 2nd Edition*, CRC Press, Boca Raton, 2013.
- 28 M. Parrinello and A. Rahman, *J. Appl. Phys.*, 1981, **52**, 7182–7190.
- 29 W. Helfrich, *Zeitschrift Für Naturforschung. Teil C: Biochemie, Biophysik, Biologie, Virologie*, 1973, **28**, 693–703.
- 30 G. Brannigan and F. L. H. Brown, *Biophys. J.*, 2006, **90**, 1501–1520.
- 31 E. G. Brandt, A. R. Braun, J. N. Sachs, J. F. Nagle and O. Edholm, *Biophys. J.*, 2011, **100**, 2104–2111.
- 32 W.K. den Otter, and S.A. Shkulipa *Biophys. J.*, 2007, **93**, 423–433.
- 33 I. V. Tetko, J. Gasteiger, R. Todeschini, A. Mauri, D. Livingstone, P. Ertl, V. A. Palyulin, E. V. Radchenko, N. S. Zefirov, A. S. Makarenko, V. Y. Tanchuk and V. V. Prokopenko, *J. Comput. Aided Mol. Des.*, 2005, **19**, 453–463.
- 34 G. Bussi, D. Donadio and M. Parrinello, *J. Chem. Phys.*, 2007, **126**, 014101.
- 35 M. P. Allen and D. J. Tildesley, *Computer simulation of liquids*, Clarendon Press, 1987.
- 36 W. H. Press, S. A. Teukolsky, W. T. Vetterling and B. P. Flannery, *Numerical Recipes in C (2Nd Ed.): The Art of Scientific Computing*, Cambridge University Press, New York, NY, USA, 1992.